ADVANCED MATERIALS TECHNOLOGIES

Supporting Information

for *Adv. Mater. Technol.*, DOI 10.1002/admt.202202039

Print-Light-Synthesis of Gold Thin Film Electrodes for Electrochemical Sensing

*Emanuela Maiorano, Stefano Gianvittorio, Massimiliano Lanzi, Domenica Tonelli, Horst Pick and Andreas Lesch**

Supporting Information

Print-Light-Synthesis of Gold Thin Film Electrodes for Electrochemical Sensing

*Emanuela Maiorano,[#] Stefano Gianvittorio,[#] Massimiliano Lanzi, Domenica Tonelli, Horst Pick, Andreas Lesch**

E. Maiorano, S. Gianvittorio, M. Lanzi, D, Tonelli, A. Lesch
University of Bologna, Department of Industrial Chemistry "Toso Montanari", Viale del Risorgimento 4, 40136 Bologna, Italy
* E-mail corresponding author: andreas.lesch@unibo.it

E. Maiorano, H. Pick
Ecole Polytechnique Fédérale de Lausanne (EPFL), Environmental Engineering Institute, GR-LUD, School of Architecture, Civil and Environmental Engineering, EPFL Station 2, 1015, Lausanne, Switzerland

# Equal contribution

S1. Instrumentation used for Print-Light-Synthesis with a combined inkjet printer and UV light source

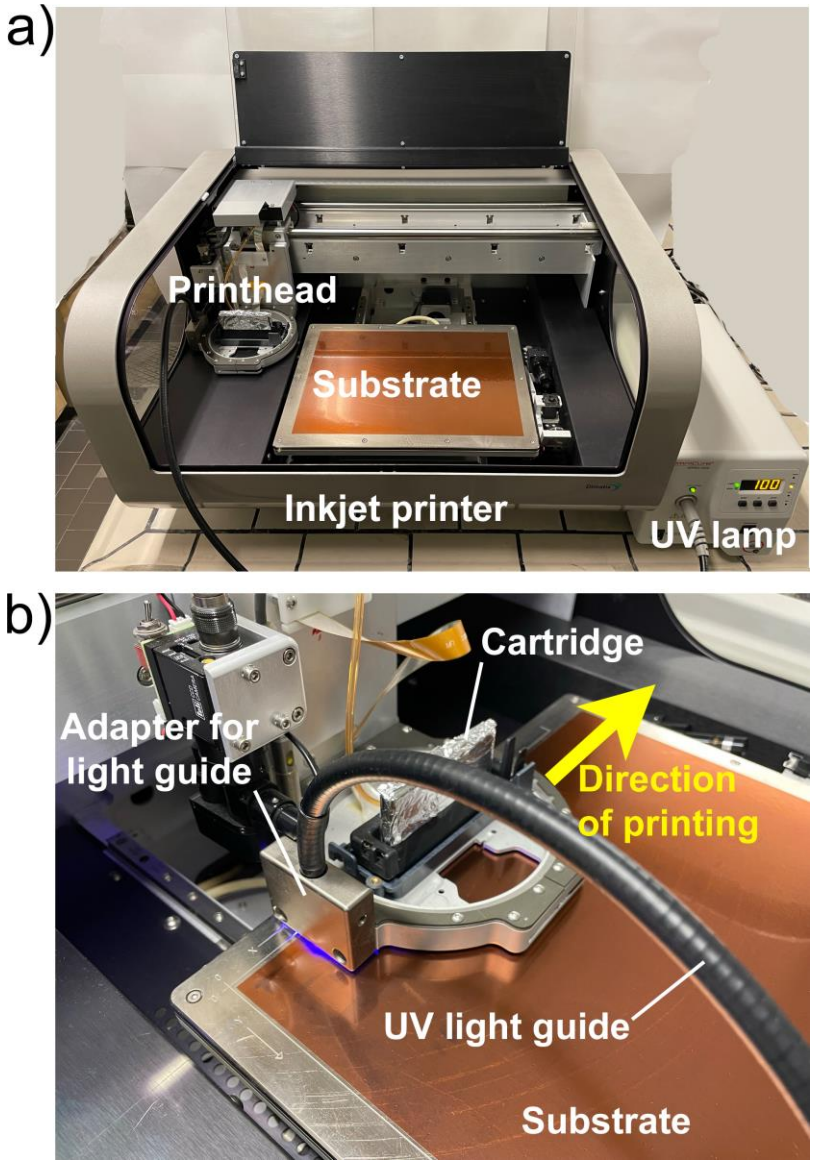

Figure S1. Photographs of the instrumentation comprising an inkjet printer combined with a UV lamp used for in-line Print-Light-Synthesis, *i.e.*, simultaneous inkjet printing and light irradiation for each printing pass (instead of a sequential process). a) Inkjet printer and UV lamp. b) Close view on the printhead carrier.

S2. Reactions during the photochemical and thermal reduction of $[AuCl_4]^-$

The photochemical and thermal reduction pathways of $[AuCl_4]^-$ are quite well known understood for diverse reactions conditions, such as light sources, light intensity, presence and absence of reducing agents, etc. In the following an overview is given about the most important reactions that are most likely involved in the PLS of Au NPs and Au films.

UV light-induced redox reactions in solution:

Relevant primary species that are created during irradiation-based reactions in the PLS ink according to literature include the hydrated electron e^-_{aq}, $H^\bullet$, $HO^\bullet$ and the isopropanol radical.[1]

$$H_2O \xrightarrow{h\nu} H^\bullet + HO^\bullet \quad \text{(S1)}$$

$$2\,H_2O \xrightarrow{h\nu} H_2O^+ + e^- + H_2O \xrightarrow{H_2O} H_3O^+ + e^-_{aq} + HO^\bullet \quad \text{(S2)}$$

$$Cl^- \xrightarrow{h\nu,\ H_2O} Cl^\bullet + e^-_{aq} \quad \text{(S3)}$$

$$\left[Au^{III}Cl_4\right]^- + (CH_3)_2CHOH \xrightarrow{h\nu} \left[Au^{II}Cl_4\right]^{2-} + (CH_3)_2C^\bullet OH + H^+ \quad \text{(S4)}$$

$$\left[Au^{III}Cl_4\right]^- + 2(CH_3)_2CHOH \xrightarrow{h\nu} \left[Au^{I}Cl_2\right]^- + 2(CH_3)_2C^\bullet OH + 2H^+ + 2Cl^- \quad \text{(S5)}$$

The reduction of $[AuCl_4]^-$ to Au^0 by direct multiphoton absorption by $[AuCl_4]^-$ has not been suggested in the literature to be a major reaction and is therefore not presented in this overview.[2].

Subsequent reactions in solution:

Based on the light-induced species there are several subsequent reactions.[1b-d, 3]

$$2\,HO^\bullet \longrightarrow H_2O_2 \quad \text{(S6)}$$

$$\left[Au^{III}Cl_4\right]^- + \frac{3}{2}H_2O_2 \longrightarrow Au^0 + \frac{3}{2}O_2 + 3H^+ + 4Cl^- \quad \text{(S7)}$$

$$H^\bullet \xrightarrow{H_2O} H^+ + e^-_{aq} \quad \text{(S8)}$$

$$\left[Au^{III}Cl_4\right]^- + 3e^-_{aq} \longrightarrow Au^0 + 4Cl^- \quad \text{(S9)}$$

$$(CH_3)_2CHOH + HO^\bullet \longrightarrow (CH_3)_2C^\bullet OH + H_2O \quad \text{(S10)}$$

$$\left[Au^{III}Cl_4\right]^- + (CH_3)_2C^\bullet OH \longrightarrow \left[Au^{II}Cl_4\right]^{2-} + (CH_3)_2CO + H^+ \quad \text{(S11)}$$

$$2\left[Au^{II}Cl_4\right]^{2-} \longrightarrow \left[Au^{III}Cl_4\right]^- + \left[Au^{I}Cl_2\right]^- + 2Cl^- \quad \text{(S12)}$$

$$\left[Au^{II}Cl_4\right]^{2-} + (CH_3)_2CHOH \longrightarrow \left[Au^{I}Cl_2\right]^- + (CH_3)_2C^\bullet OH + H^+ + 2Cl^- \quad \text{(S13)}$$

$$\left[Au^{I}Cl_2\right]^- + (CH_3)_2C^\bullet OH \longrightarrow Au^0 + (CH_3)_2CO + H^+ + 2Cl^- \quad \text{(S14)}$$

$(Au^0)_n$ indicates the generation of Au^0 assemblies forming eventually Au clusters.

$$\left(Au^0\right)_n + \left[Au^{I}Cl_2\right]^- + \left(CH_3\right)_2 C^{\bullet}OH \longrightarrow \left(Au^0\right)_{n+1} + \left(CH_3\right)_2 CO + H^+ + 2Cl^- \quad (S15)$$

$$\left(Au^0\right)_n + \left(Au^0\right)_m \longrightarrow \left(Au^0\right)_{n+m} \quad (S16)$$

$$\left(Au^0\right)_n + \frac{3}{2}H_2O_2 + \left[Au^{III}Cl_4\right]^- \longrightarrow \left(Au^0\right)_{n+1} + \frac{3}{2}O_2 + 3H^+ + 4Cl^- \quad (S17)$$

The contribution of $H^{\bullet}$ to the reduction of $[AuCl_4]^-$ is negligible, because the $H^{\bullet}$ quenching reactions are faster than the diffusion-controlled reaction with $[AuCl_4]^-$.[1c] In any case, these radicals can be scavenged by the alcohols present in the reaction mixture.

The hydrated electron can be quenched by the following reactions.[4]

$$2e^-_{aq} + 2H_2O \longrightarrow H_2 + 2OH^- \quad (S18)$$

$$e^-_{aq} + H^{\bullet} + H_2O \longrightarrow H_2 + OH^- \quad (S19)$$

$$e^-_{aq} + HO^{\bullet} \longrightarrow OH^- \quad (S20)$$

$$e^-_{aq} + O_2 \longrightarrow O_2^- \quad (S21)$$

Further role of isopropanol and 1,2-propanediol:

Isopropanol and 1,2-propanediol scavenge the radicals $^{\bullet}OH$ and $^{\bullet}H$, and H_2O_2, which is an advantage as those species could also reversibly oxidize Au.[1b, 5]

Thermally induced redox reactions at air:

Three particular steps at three temperature ranges are generally reported in literature.

Step 1:

$$HAu^{III}Cl_4 \cdot 3H_2O_{(l)} \xrightarrow{75\text{–}180^{\circ}C} Au^{III}Cl_{3(s)} + HCl_{(g)} + 3H_2O_{(g)} \quad (S22)$$

$$HAu^{III}Cl_4 \cdot 3H_2O_{(l)} \xrightarrow{75\text{–}180^{\circ}C} HAu^{III}Cl_2\left(OH\right)_{2(s)} + 2HCl_{(g)} + H_2O_{(g)} \quad (S23)$$

Step 2:

$$Au^{III}Cl_{3(s)} \xrightarrow{180\text{–}235^{\circ}C} Au^{I}Cl_{(s)} + Cl_{2(g)} \quad (S24)$$

$$HAu^{III}Cl_2\left(OH\right)_{2(s)} \xrightarrow{180\text{–}235^{\circ}C} Au^0 + 2HCl_{(g)} + \frac{1}{2}H_2O_{(g)} + \frac{3}{4}O_{2(g)} \quad (S25)$$

Step 3:

$$2Au^{I}Cl_{(s)} \xrightarrow{235\text{–}320^{\circ}C} 2Au^0_{(s)} + Cl_{2(g)} \quad (S26)$$

S3. Absorption spectra of the Au precursor ink and polyimide substrate

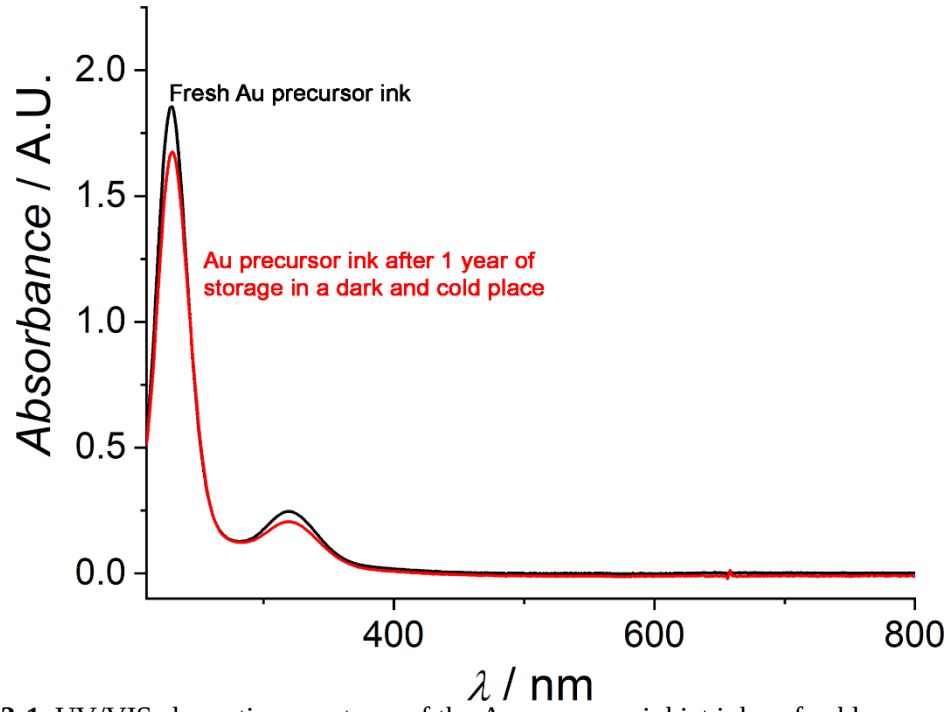

Figure S3-1. UV/VIS absorption spectrum of the Au precursor inkjet ink as freshly prepared (black curve) and after 12 months of storage (red curve) in a cold and dark place. No absorbance is recordable that could be related to Au NPs.

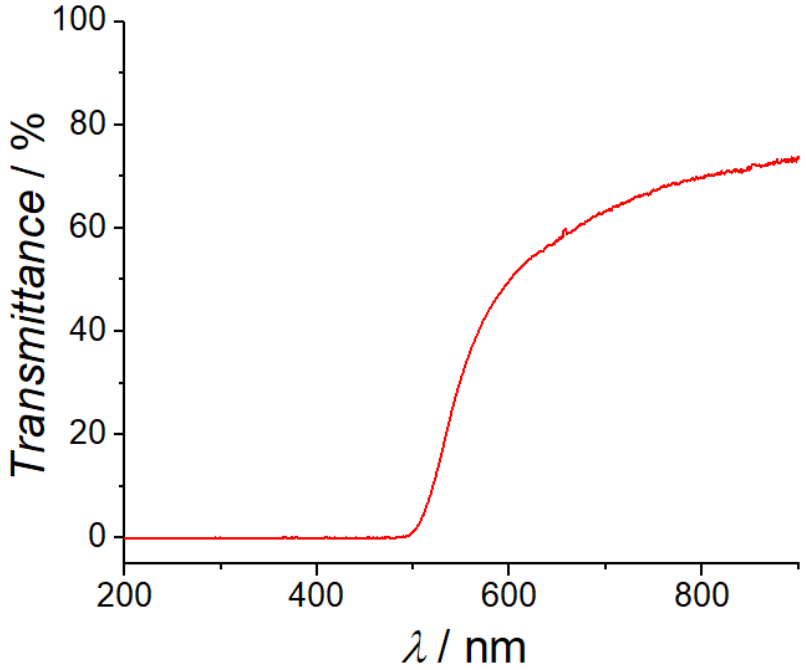

Figure S3-2. UV/VIS absorption spectrum of the polyimide substrate used in this work. Shown as transmittance%.

S4. Print-Light-Synthesis of Au films on glassy carbon plate and indium-tin oxide-coated glass slide

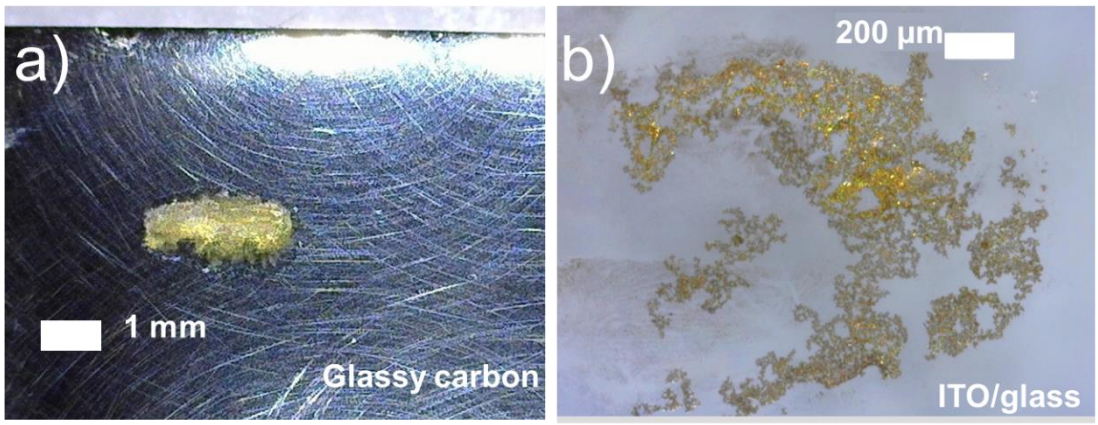

Figure S4. Au films prepared by PLS on glassy carbon (rapid heat transfer away from the reaction zone) and on ITO/glass (no light absorption by the substrate that consequently does not heat up). Printing parameters were identical to the ones described in the main manuscript. These results demonstrate that heat generating by the substrate through absorption of UV irradiation is not the main cause for Au precursor reduction to Au^0.

S5. Resistance measurements

The resistances of the solid Au films were measured using a Four-Point-Probe measurement system, in which the four probes were collinearly oriented and placed on the surface of the center of the Au films. The current flowing between the outer two tips was controlled and the resulting voltage drop measurement between the two inner probes. The electrical conductivity was calculated following the theory for a thin, rectangular slice on an insulator as developed by Smits and Topsoe. This is schematically shown for a gold film (yellow) on PI (brownish-reddish) in **Fig. S5-1** where s is the probe spacing, t_{Au} is the thickness of the solid Au film, either measured by SEM or calculated using the calibration equation obtained by linear regression of a series of SEM images, a_{Au} is the length of the solid film and b_{Au} is the width of the solid Au film.

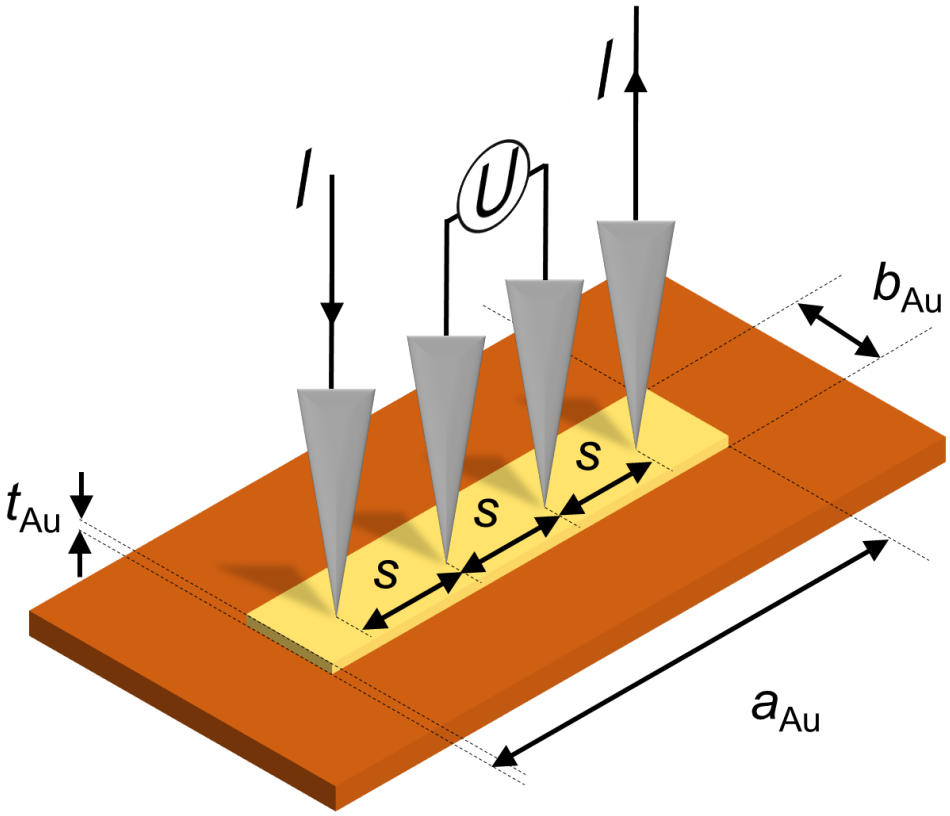

Figure S5-1. Schematic representation of arrangement of the probes and considered dimensions for the Four-Point-Probe measurements to obtain the resistances of the solid Au films.

The resistivity ρ is given by **Eq. S27**:

$$\rho = \frac{U}{I} \cdot G = R \cdot \frac{\pi}{\ln 2} \cdot C = R \cdot 4.5324 \cdot C \quad [\Omega \cdot \mathrm{m}] \tag{S27}$$

Where $G = t \cdot \pi/(\ln 2)$ is the geometric factor for an infinitely large slice with a thickness t much smaller than the probe spacing s. G contains further correction factor C that must be applied because of the finite rectangular shape of the film to be measured. C values are tabulated and were taken for each pattern analyzed. For instance, with a probe spacing s = 1 mm and with film width b_{Au} = 2 mm, C is 0.4297 independent of the ratio a_{Au}/b_{Au}. U the measured voltage and I the applied current.

The electrical conductivity can then be calculated by using **Eq. S28**:

$$\sigma = \frac{1}{\rho} \quad [\mathrm{S/m}] \tag{S28}$$

The thickness of the solid Au films was measured from SEM images of the cross-sections of the Au films that were obtained by mechanical cutting using a razor blade. The thickness was linear as a function of the Au loading. By linear regression with fixed zero as intercept the following calibration graph and equation was obtained. The data are shown in **Table S5-1**.

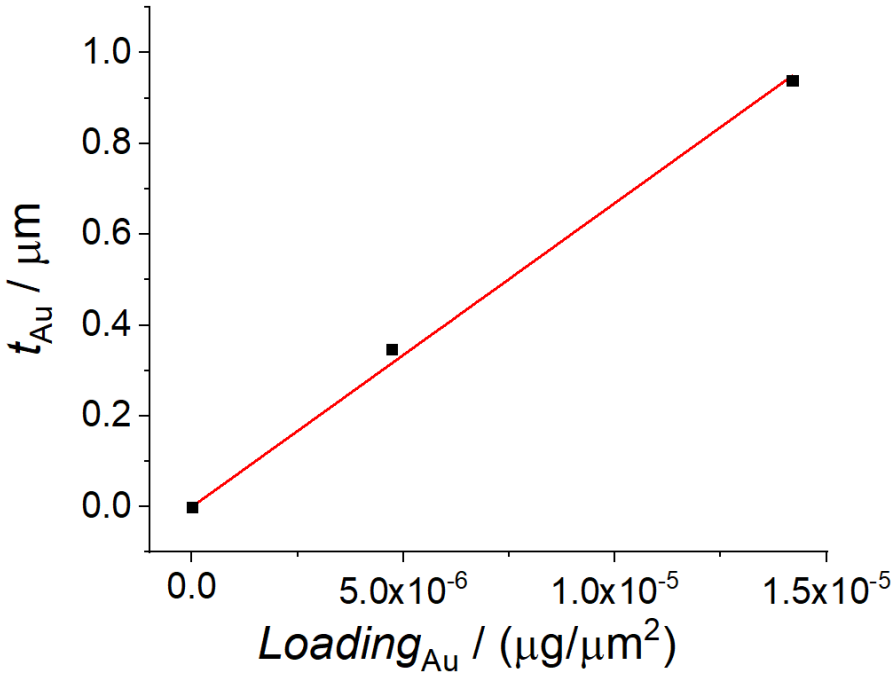

Figure S5-2. Calibration graph of the thickness of the Au film as function of the printed Au loading.

$$t_{Au}\ (\mu m) = 6.69\times10^4\ \mu m^3/\mu g \cdot loading_{Au}\ (\mu g/\mu m^2) \tag{S29}$$

Table S5-1. Loading and density of Au films obtained by Print-Light-Synthesis

$Loading_{Au}$ (µg/cm^2)	t_{Au} (µm)*	$Density_{Au}$ (g/cm^3)	*%density of bulk Au*[#]
472	0.347	13.60	70
1419	0.939	15.11	78

* thickness from SEM measurements of the cross-section of the Au films obtained by blade cutting
[#] the density of bulk Au is 19.32 g/cm^3

The comparison with the electrical conductivities of Au films that were prepared by using similar technologies and Au precursors, but also Au nanoparticle inks for inkjet printing are demonstrated in **Table S5-2**. The difference in electrical conductivity of our Au film in respect to bulk Au could also be caused or at least influenced by the measured thickness of the Au films by using SEM of the Au film cross-sections. Indeed, the cross-section was created by razor blade cutting that could slightly deform the Au film giving the impression of a thicker gold layer. Nevertheless, the PLS Au films are in the order of bulk Au and comparative gold films.

Table S5-2. Comparison of the Au films obtained by Print-Light-Synthesis with a selection of other Au films obtained by inkjet printing and/or photochemical deposition approaches

Method	Metal source	Process conditions	Electrical conductivity (×10^7) S/m	%Electrical conductivity bulk gold*	Reference
IJP	Au inorganic precursor ink	Photochemical (UV)	0.72	16	This work
IJP	Au-organic precursor	Thermal (280 °C)	1.9	43	[6]
IJP	Protected Au NPs	Thermal (500 °C)	0.80	18	[7]
IJP	Functionalized Au NPs	Thermal (220 °C)	1.0	23	[8]
IJP	Functionalized Au NPs	Thermal (150 °C)	0.3	7	[9]
APD	Au inorganic precursor ink	Photochemical (UV)	1.08	25	[10]
PSL-PPD	Au inorganic precursor with citrate, oxalate and poly(allylamine)	Photochemical (UV)	N/A	N/A	[11]

LPP	Au inorganic precursor ink	Photochemical (laser 445 nm)	N/A	N/A	[12]
DLP	Au inorganic precursor ink	Photocatalytic on TiO_2 (UV)	N/A	N/A	[13]
DLP	PVD Au	Etching by UV generating cyanide anions	N/A	N/A	[14]
Dip coating	Au inorganic precursor ink with micelle templating	Photochemical (UV)	N/A	N/A	[15]
DLW	Au inorganic precursor ink	Photochemical (laser 405 nm) + electrochemical	N/A	N/A	[16]

* Electrical conductivity of bulk gold $4.4 \cdot 10^7$ m/s [17]

APD - Anion-assisted photochemical deposition
DLP – Digital light processing
DLW - Direct laser writing
IJP - Inkjet printing
LPP - Laser Projection Printing
PSL-PPD - Projection stereolithography with polymer-assisted photochemical deposition
PVD – Photochemical vapor deposition

S6. Cyclic voltammogram using a screen-printed graphite electrode coated with gold nanoparticles

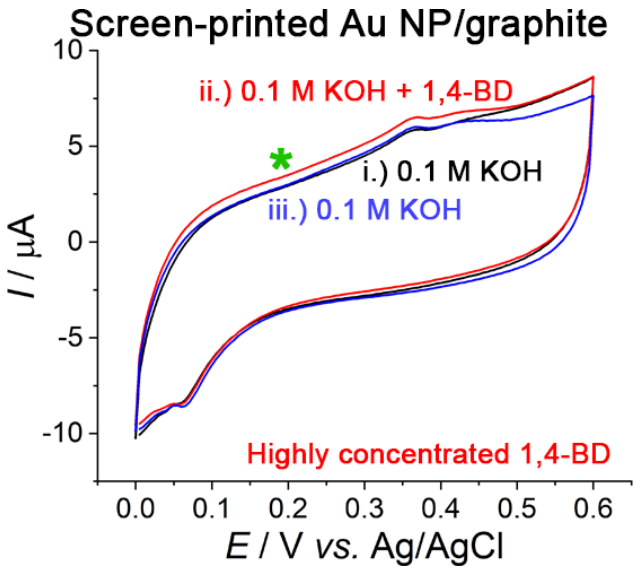

Figure S6. Application performance of a standard screen-printed Au NP electrode with graphite as conductive base material in absence and presence of the analyte 1,4-butanediol in 0.1 M KOH. CVs in i.) 0.1 M KOH (black curves), ii.) 0.1 M KOH with high concentration of 1,4-BD (red) and iii.) again in 0.1 M KOH (blue); potential scan rate 100 mV/s; CE and RE as in Figure 7 of the main manuscript.

S7. Fully inkjet-printed three-electrode sensor comprising PLS Au

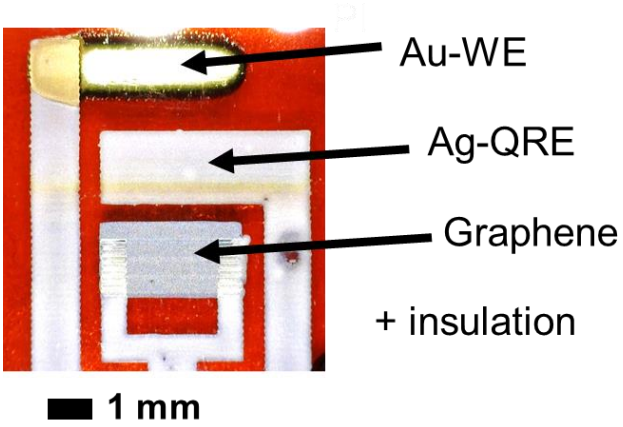

Figure S7. Example of a fully inkjet printed sensor comprising PL Au as working electrode (WE), graphene as counter electrode (CE) and Ag as quasi reference electrode (QRE) and material for the electric traces. Photo taken before printing the insulation ink.

References

[1] a) D. N. Nikogosyan, A. A. Oraevsky, V. I. Rupasov, *Chem. Phys.* **1983**, *77*, 131-143; b) E. Gachard, H. Remita, J. Khatouri, B. Keita, L. Nadjo, J. Belloni, *New J. Chem.* **1998**, *22*, 1257-1265; c) V. K. Meader, M. G. John, C. J. Rodrigues, K. M. Tibbetts, *J. Phys. Chem. A* **2017**, *121*, 6742-6754; d) X. Liu, X. Zhang, D. Khakhulin, P. Su, M. Wulff, F. Baudelet, T. C. Weng, Q. Kong, Y. Sun, *J. Phys. Chem. Lett.* **2022**, *13*, 8921-8927.

[2] B. Tangeysh, K. Moore Tibbetts, J. H. Odhner, B. B. Wayland, R. J. Levis, *J. Phys. Chem. C* **2013**, *117*, 18719-18727.

[3] M. Harada, S. Kizaki, *Cryst. Growth Des.* **2016**, *16*, 1200-1212.

[4] N. Nakashima, K. I. Yamanaka, M. Saeki, H. Ohba, S. Taniguchi, T. Yatsuhashi, *J. Photochem. Photobiol., A* **2016**, *319-320*, 70-77.

[5] L. M. Frias Batista, V. K. Meader, K. Romero, K. Kunzler, F. Kabir, A. Bullock, K. M. Tibbetts, *J. Phys. Chem. B* **2019**, *123*, 7204-7213.

[6] C. Schoner, A. Tuchscherer, T. Blaudeck, S. F. Jahn, R. R. Baumann, H. Lang, *Thin Solid Films* **2013**, *531*, 147-151.

[7] W. Cui, W. Lu, Y. Zhang, G. Lin, T. Wei, L. Jiang, *Colloids Surf. A: Physicochem. Eng. Asp.* **2010**, *358*, 35-41.

[8] S. Mekhmouken, N. Battaglini, G. Mattana, A. Maurin, S. Zrig, B. Piro, D. Capitao, V. Noel, *Electrochem. Commun.* **2021**, *123*.

[9] J. Im, G. F. Trindade, T. T. Quach, A. Sohaib, F. Wang, J. Austin, L. Turyanska, C. J. Roberts, R. Wildman, R. Hague, C. Tuck, *ACS Applied Nano Materials* **2022**, *5*, 6708-6716.

[10] D. Wu, B. Yao, S. Wu, H. Hingorani, Q. Cui, M. Hua, I. Frenkel, Y. Du, T. K. Hsiai, X. He, *Adv. Mater.* **2022**, *34*.

[11] Z. Zhao, J. Bai, Y. Yao, C. Wang, *Mater. Today* **2020**, *37*, 10-17.

[12] X. Wang, K. Cui, Q. Xuan, C. Zhu, N. Zhao, J. Xu, *ACS Appl. Mater. Interfaces* **2019**, *11*, 21668-21674.

[13] Y. Zhang, Z. Liang, A. P. Zhang, H. Y. Tam, *Adv. Opt. Mater.* **2021**, *9*.

[14] M. Gregorini, R. N. Grass, W. J. Stark, *Ind. Eng. Chem. Res.* **2020**, *59*, 12048-12055.

[15] F. Kundrat, G. Baffou, J. Polleux, *Nanoscale* **2015**, *7*, 15814-15821.

[16] C. Rosenbaum, M. Murphy, P. T. Lawrence, C. Sirkoch, S. R. Schneeberg, K. Zigner, S. Morris, E. Richman, C. Anyanwu, E. Will, C. Wheeler, E. Reed, C. N. Lafratta, *Int. J. Extreme Manuf.* **2022**, *4*.

[17] D. R. Lide, *CRC Handbook of Chemistry and Physics*, 92nd Ed. ed., CRC Press, **2011**.